# Coupling of Bound States to Continuum States in Neutral Triatomic Hydrogen

H. Helm, U. Galster, I. Mistrik, U. Müller, and R. Reichle
*Department of Molecular and Optical Physics, Universität Freiburg, Fakultät für Physik, Hermann-Herder-Str. 3, D-79104 Freiburg, Germany*

**Abstract**: Excited states of neutral $H_3$ in the vicinity of the ionization threshold are resonances in the dissociative recombination (DR) process, $H_3^+ + e \rightarrow H + H_2$ and $H_3^+ + e \rightarrow H + H + H$. Over the past twenty years a great amount of experimental data on the dynamics of excited neutral triatomic hydrogen has been collected. While access from excited states of $H_3$ into the ionization continuum is now well understood in terms of multichannel quantum defect theory (MQDT), the competing access into the dissociative continua $H + H_2$ and $H + H + H$ has currently no firm theoretical explanation. This lack of understanding lies at the heart of our inability to predict and understand the very high rates observed for DR of $H_3^+$ at low electron energy.

**Key words**: DR, predissociation, autoionization

## 1. INTRODUCTION

Rydberg states of the neutral triatomic hydrogen molecule can be viewed as an electron attached to a tightly bound $H_3^+$ core [1-4]. These states are embedded in the dissociation continuum of the repulsive electronic ground state surface as seen from Figure 1. As a consequence, all excited bound states of $H_3$ are subject to predissociation. The metastable $2p\mathrm{A}_2''$(N=K=0) state is a notable exception. Here N refers to the total angular momentum apart from spin and K to the projection of N on the molecular top axis. This lowest rotational level is long-lived (700 ns) [5] owing to symmetry forbidden coupling with the electronic ground state by either radiation or predissociation. Neutral $H_3$ in this rotational level can be selectively

prepared in a fast beam by charge exchange techniques. This state has been used as a platform for laser-excitation experiments [3-14] to explore the structure and dynamics of highly excited states of $H_3$.

Some of these investigations have addressed the dissociation dynamics of state-selected low principal quantum number ($n=2,3$) Rydberg states into the fragments $H + H_2$ [13-16] as well as their three-body breakup into three ground state hydrogen atoms [17,18]. In the latest version of these experiments correlation maps of the ground state atom momentum vectors are obtained. These maps provide the most direct view of how the neutral triatomic species enters into the neutral dissociation continuum at molecular distances and how it emerges from this continuum at the separated atom limit.

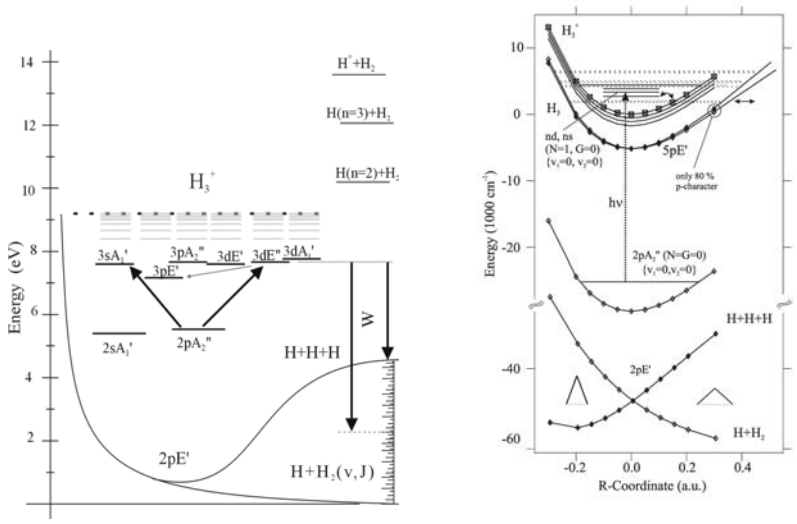


*Figure 1.* The excimer states of the $H_3$ molecule, embedded in the repulsive ground state are shown on the left. Also indicated is the translational energy release, $W$, which appears in the center-of-mass motion of the fragments when a selected state predissociates into neutral products. The figure on the right shows a cut through the potential energy surfaces. The symbols give calculated energies of the $H_3^+$ ion and of the $2p$E′, $2p$A$_2$", and $5p$E′ states of $H_3$. The $R$ coordinate corresponds to a set of asymmetric stretch geometries (see Ref. [14]).

In separate studies high principal quantum number $s$-, $p$-, $d$-, and $f$-Rydberg states were excited by one- and two-color. The rotational, vibrational, and vibronic coupling mechanisms between the Rydberg electron and the ion core were studied theoretically in $MQDT$ models [14,19,20]. Quantitative comparisons between experiment and theory indicate that with only few exceptions the level-positions and level-widths are precisely accounted for by an $MQD$ theory, which is based solely on *ab-*

*initio* parameters from quantum-chemistry calculations, without regard of the neutral dissociation continuum. Exceptions appear for selected electronic states in that their lifetime is shortened due to predissociation. The experiments indicate that selective coupling to the dissociation continuum is effective for even very high principal quantum number Rydberg states (for example at the energy of $n=61$). The exact predissociation mechanisms of Rydberg states of $H_3$ with principal quantum numbers $n>3$ are currently not well understood.

We had previously pointed out [21] that predissociated Rydberg states may play an important role in supporting the dissociative recombination (DR) process of $H_3^+$ ions. The puzzling magnitude of the DR cross section which numerous experimenters have observed at low electron energy is still at odds with theory, after substantial efforts from theory and experiment to clarify the situtation. The very latest measured cross section for DR [22] is approximately two to four orders of magnitude higher than current theory, which includes direct and indirect DR channels [23] or the Jahn-Teller coupling of *p*-states [24].

While this paper cannot pinpoint the exact origin of the failure of theory to account for the huge cross section through which low energy electrons see the open neutral continuum, it discusses several examples of state-selective predissociation and competition between predissociation with autoionization. These results are equally lacking theoretical explanation. Obviously these resonances are examples of intermediate neutral states, which are active in the DR-process. We are confident that a common explanation for their predissociation and for the fast rate of DR of low energy electrons exists.

## 2. POTENTIAL ENERGY SURFACES

In its ground vibrational level the electronic state of $H_3^+$ is best described in $D_{3h}$ geometry. The corresponding neutral excimer states of $H_3$ are shown in the center of Figure 2. What is important for DR is that all excited state dissociation limits of the neutral molecule lie energetically *above* the lowest energy of the molecular ion. It is evident from Figure 1, that any DR process involving electrons with energies less than 0.5 eV can only access the neutral electronic ground states of $H+H_2$ or $H+H+H$. In linear geometry the repulsive $1^2\Sigma_g^+$ state of $H_3$ intersects all bound excimer states, hence providing a convenient path for predissociation (Figure 2, left). This channel is closed in $D_{3h}$ geometry. Approximately 2 eV of vibrational excitation are required to open the triangular configuration of the ion into linear geometry in order to directly enter the continuum. Obviously tunneling will permit access at significantly lower energy, however no quantum chemistry

calculations are currently available to estimate the likelyhood of tunneling. Quantum chemistry calculations of the potential energy surfaces at geometries intermediate to these shown in Figure 2 would help estimate such effects.

Fig. 2 only shows the energy levels of doublet $H_3$, as appropriate for addition of one electron to ground-state singlet $H_3^+$. Quartet states of $H_3$ also exist, however the vertical energy separation of triplet $H_3^+$ from the ionic ground state geometry is about *20 eV* [25]. Hence quartet states should play no role in the dynamics of $H_3$ near its lowest ionization threshold. The electronically excited doublet states (except for the repulsive *2p*E' ground state surface) can be viewed as Rydberg states with a tightly bound $H_3^+$ core [4]. The equilibrium geometry of the ion, as well as the neutral excimers, is that of an equilateral triangle. Owing to the fermionic nature of particles forming $H_3^+$ only odd rotational levels exist for $K = 0$ for the nondegenerate vibrational levels [26].

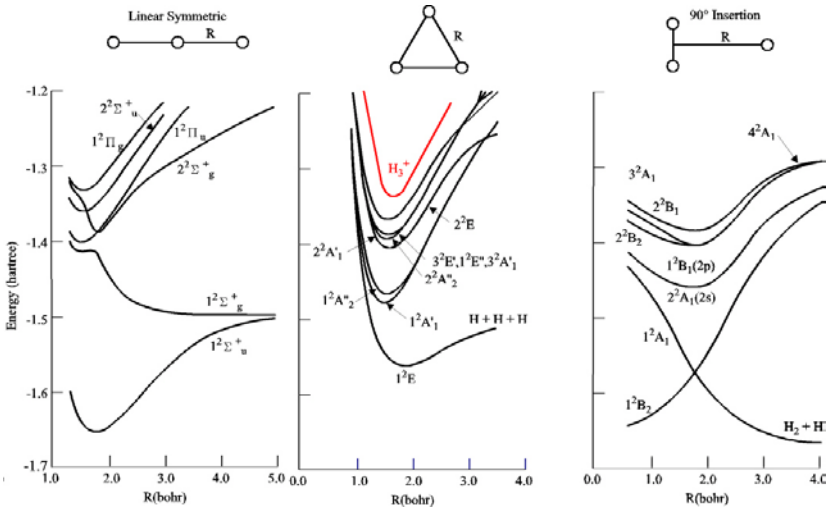


*Figure 2.* Energy levels of the $H_3$ molecule for three configurations are compared on an absolute energy scale (taken from Ref. [27]). The meaning of the $R$ -coordinate is indicated in the figure above each diagram.

The Rydberg states of $H_3$ are labelled [19] by $nL\Gamma$ (N,G)$\{\nu_1,\nu_2^{\iota}\}$. These states are characterized by the principal quantum number $n$, the electronic angular momentum $L$ of the Rydberg electron, and the electronic symmetry $\Gamma$ in the $D_{3h}$ group. The nuclear vibrational motion is labelled by the quantum numbers of the symmetric stretch ($\nu_1$) and degenerate ($\nu_2$) modes, and the vibrational angular momentum $\iota$. The molecular rotation is described by the total angular momentum $N$ disregarding electron spin, its projection

on the molecular top axis *K*, and Hougen's convenient quantum number [28] $G = \iota + \lambda - K$.

## 3. PREDISSOCIATION

Experimentally known lifetimes of the lower-lying Rydberg states are collected in the table below. For references see Table I of Ref. [29]. As is evident from the magnitude of the lifetimes predissociation is a major decay channel of these states.

| electronic state label $nL\Gamma$ | rovibrational state label (N,G){$\nu_1,\nu_2^{\iota}$} | experimental lifetime [ps] | theoretical lifetime [ps] | state energy relative to $H_3^+$ [eV] |
|---|---|---|---|---|
| $2s$A$_1$' | (1,0){0,0$^0$} | 0.2 | 1.7 | -3.777 |
| $3s$A$_1$' | (1,0){0,0$^0$} | 1000 | 8000 | -1.595 |
| $4s$A$_1$' | (1,0){0,0$^0$} | 7.6 | - | -0.885 |
| $5s$A$_1$' | (1,0){0,0$^0$} | 4.4 | - | -0.562 |
| $3p$E' | (1,0){0,1$^1$} | >66 | 39 | -1.737 |
| $3s$A$_1$' | (1,0){1,0$^0$} | >66 | 1400 | -1.197 |
| $4p$E' | (1,0){0,1$^1$} | 21 | - | -0.714 |
| $5p$A$_2$" | (2,0){0,2$^2$} | 6 | - | 0.034 |
| $20p$E' | (2,0){1,0$^0$} | 5 | - | 0.369 |
| $6d$E" | (1,0){1,0$^0$} | 2 | - | 0.014 |

Experiments observe a most dramatic variation in lifetime among the *s*-states at low values of *n*. The lifetime increases by almost four order of magnitude when going from *n=2* to *n=3,* but decreases again by two orders of magnitude from *n=3* to *n=4.* A recent theoretical study based on vibronic coupling between *ns* states with the ground *2p*E' state [30] is able to explain the ratio of lifetimes between *2s* to *3s* in terms of the reduced overlap of the *3s* potential energy surface with the repulsive ground state. However the experimental result that the coupling is again more efficient for the higher lying *4s* and *5s* states cannot be accounted for. The surfaces of the higher *n*-states are further removed from the repulsive ground state, hence having weaker overlap. We note that the avoided crossing between the repulsive $1^2\Sigma_g^+$ state of $H_3$ and the bound excimer states (see Figure 2 left) falls energetically between the lowest vibrational levels of the *3s* and the *4s* state and may play a role in the predissociation of the higher lying *s*-states.

The *np*E' states are homogeneously coupled to the ground state surface. No theoretical data on their predissociation lifetimes exist. Such results could be obtained using the formalism presented by Greene *et al.* [24]. The lifetimes of the *np*A$_2$" levels are governed by rotational coupling with the ground electronic state. The lifetime should decrease with $N(N+1)-K(K+1)$,

as has been observed for the $2p\mathrm{A}_2$" state [2]. For the vibrationally excited *5p, 20p* and *3d* states autoionization competes with predissociation, both operating in the time scale of a few picoseconds.

## 3.1 Predissociation of high-n Rydberg states

High principal quantum number Rydberg states (*n>30*) were investigated by monitoring both the field ionization signal concurrent with the photofragment yield [29]. In Fig. 3 the photofragment yield [3a and 3b] is shown as well as the field ionization signal [3c], following one-photon excitation from the $H_3$ $2p\mathrm{A}_2$" state in the energy range just below the lowest ionization threshold.

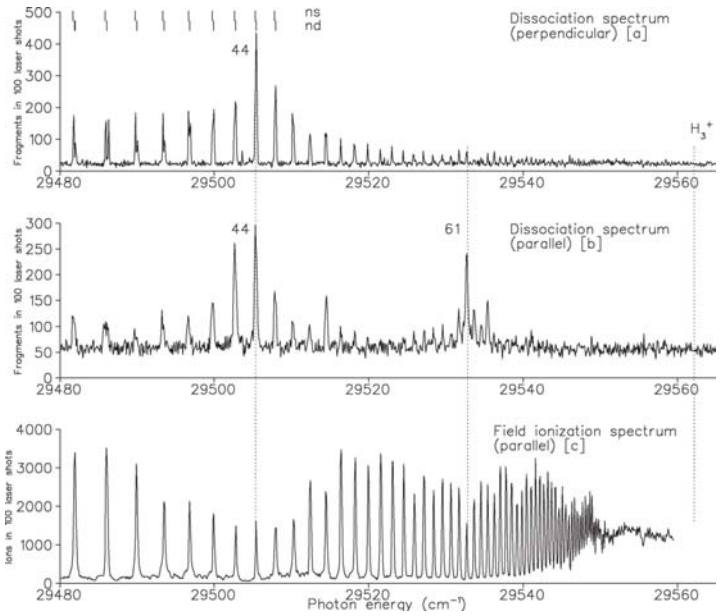


Figure 3. Laser-excitation of $H_3$ in the vicinity of the lowest ionic limit. The photofragment yield [a,b] is compared with the field ionization spectrum [c]. In [a], the laser polarization was perpendicular, in [b] parallel to the axis defined by the lateral displacement of the detector for neutral fragments. The *ns*- and *nd*-Rydberg series converging to the $H_3^+(1,0)\{0,0^0\}$ threshold are indicated by tickmarks.

The transitions in the ionization spectrum were assigned to the *d*-Rydberg series converging to the $H_3^+(1,0)\{0,0^0\}$ threshold [3] which is marked by a dashed line. Up to the highest resolved principal quantum numbers, contributions also appear in the photofragment signals.

The windows in the field ionization intensity close to *n=44* and *n=61* correlate with enhanced fragment yield. An earlier laser depletion

experiment [13] showed that the absorption strength is a monotonous function of principle quantum number. The intensity modulations which appear in Figure 3c are caused by a shortening of the lifetime due to predissociation. In the experiment only an upper limit can be ascertained for the lifetime of the states, which appear in the spectra of Figure 3. The Rydberg states predissociate on a time scale faster than about $2\mu s$. The significantly different magnitude of the photofragment signal observed for the two orientations of the laser polarization relative to the detection-axis (Figure 3a and 3b) is caused by the state specific angular distribution of photofragments. When perpendicular laser polarization is chosen, the photodissociation signal in the vicinity of $n=44$ is significantly larger than that at $n=61$. This suggests that the doorway states mediating the predissociation process are different in nature at $n=44$ and $n=61$. This is consistent with the observation of a profound electric field dependence of the intensity window at $n=61$. Predissociation of the $61d$-state is due to Stark mixing [12] with a vibrationally excited member of the $np$E′ series. In contrast the predissociation doorway around $n=44$ is insensitive to the presence of external electrical fields, hence this state must find access to the neutral continuum via another doorway state. In addition to the interlopers at $n=44$ and $n=61$, increased predissociation is observed in the vicinity of the $n=14$ and $n=21$ states.

It is remarkable that $ns$-Rydberg members are observed in the photofragment signal in Figure 3, while they are absent in the ionization signal. This shows that the $s$-series members are much more strongly predissociated that are higher $L$-states. The energetic location of most members of the $s$- and $d$-series are in agreement with the Rydberg formula using the established quantum defects to a precision of 0.2 $cm^{-1}$. However, perturbations which shift the line positions by more than 0.5 $cm^{-1}$ appear at $13d$, $14d$, and $24s$. A number of additional predissociating resonances built on vibrationally excited cores of $H_3^+$ have also been identified (see Table II of ref. [29]).

## 3.2 Predissociation of autoionizing Rydberg states

In the $p$E'-series built on a symmetric-stretch excited $H_3^+$ core, the positions, relative amplitudes, and widths of most of the quasi-discrete lines are generally understood from an $MQD$-theory which does not take into account the existence of the neutral dissociation continuum. For a few members of the series, the measured relative intensities are observed to be lower and the line widths broader than those predicted by $MQDT$. This observation was taken as indication that predissociation competes with autoionization.

The autoionization and predissociation spectrum in the range from 369.46 to 370.20 *meV* above the ionization threshold is shown in Fig. 4e and 4f, respectively. This range covers the vicinity of the $20p\{1,0^0\}$ states with $N=1$ and $N=2$, excited via the $3sA_1'(1,0)\{1,0^0\}$ intermediate. Taking into account the geometric collection efficiency of the off-axis detector which we find that the branching between predissociation and autoionization for the $N=2$ state amounts to at least 25%. Apparently, the $N=2$ state is strongly predissociated while the decay of the $N=1$ state is dominated by autoionization.

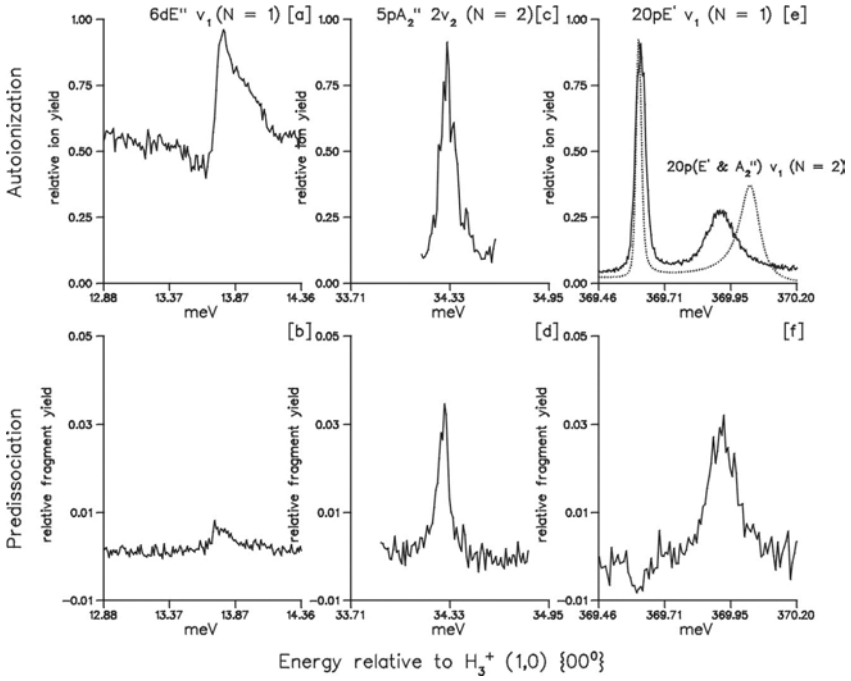


Figure 4. Examples of spectra, which reveal that predissociation competes with autoionization above the first ionization threshold of $H_3$. The dotted curve gives the *MQDT* prediction.

As an example for a *d*-state, we have investigated the symmetric-stretch excited $6d$E''$(1,0)\{1,0^0\}$ state of $H_3$ which can be excited in a one-photon transition. The corresponding autoionization and predissociation spectra are shown in Fig. 4a and 4b. The Fano-type shape of the line profile is caused by the interference with the underlying ionization continuum. The decay of the $6d$E'' state is dominated by autoionization, the branching into predissociation is of the order of only a few percent. A third example where predissociation competes with autoionization is the $5p\mathrm{A}_2''(2,0)\{0,2^0\}$ level shown in Fig. 4c and 4d. Also here the branching to predissociation amounts to a few percent.

As is evident from the energy scales in Figure 4, low energy electrons involved in DR will find such states in the collision continuum and thereby gain access to the neutral ground state continuum.

## 3.3 Three-body decay

Predissociation lifetimes and the branching between predissociation and other decay channels are important experimental data to illucidate the dynamics of $H_3$. Additional experimental information can be gained on how the neutral molecule finds access into the dissociative continuum. Such information is contained in the dissociation products. For the states investigated here, as well as for the products of low energy DR, the final states are always in their ground electronic state, $H+H_2$(v,J) or else three hydrogen atoms, $H(1s)+H(1s)+H(1s)$. In the former case the total energy available is shared between the translational energies of the atomic and the molecular fragment and the rovibrational excitation of the $H_2$ product.

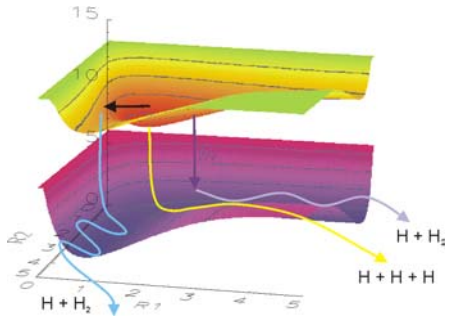


Figure 5: Schematic paths of predissociation into the repulsive ground state surface of $H_3$. The upper Jahn Teller sheet of the ground state surface which branches to the $H+H+H$ limit (see Figure 2, left) is not shown. The origin of vibrational excitation of the $H_2$ product is apparent from the decay path on the left.

It is obvious from Figure 5 that the degree of rovibrational excitation is governed by the exact shape of the trough of the repulsive ground state surface and the initial position of the wavepacket when it enters this surface. In this sense the shape of the initial wavepacket disperses among the trajectories which populate specific (v,J) combinations [30]. In the case of two-body decay the information on the actual coupling to the neutral continuum, combined with the dynamic evolution on the ground state surface, is cast into a complex set of (v,J) variables, which bar us from a direct view of the predissociation mechanism.

The situation is intrinsically different in case of three-particle decay. Here, the sum of the kinetic energy of the three fragments is fixed at the

energy difference *W* between the excited state and the *H(1s)+H(1s)+H(1s)* limit. In this case the balanced center-of-mass momentum vectors in the molecular state are directly imaged into macroscopic observables: the correlated set of the three momentum vectors at which the framents appear in the laboratory frame. A direct analysis of the three correlated momentum vectors is possible with the photofragment spectrometer developed at Freiburg [18]. With this instrument triple coincidences of *H+H+H* are collected on a multi-hit time- and position-sensitive detector. The individual vectorial momenta of the three hydrogen atoms $m\mathbf{u}_1$, $m\mathbf{u}_2$, and $m\mathbf{u}_3$ in the center-of-mass frame are determined separately and a consistency check that $W = ( m\mathbf{u}_1^2 + m\mathbf{u}_2^2 + m\mathbf{u}_3^2 )/2$ can be carried out for each individual molecule investigated. Momentum conservation requires that $\mathbf{u}_1+\mathbf{u}_2+\mathbf{u}_3=0$. This implies that the three vectors have only six independent components. Given the experimental information on the three individual vectors we can determine the 6-fold differential cross section, completely characterizing the final state of the three-body decay process.

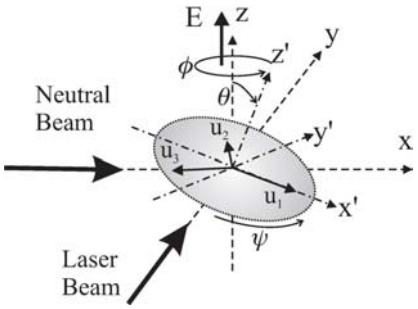


Figure 6: Orientation of the fragment momentum vectors in a three-body decay process.

In order to gain insight into the fragmentation pattern, we consider suitable projections of this six-dimensional set of information. We introduce the parameters in Figure 6, which uniquely describe the three fragment momentum vectors. The $\mathbf{u}_i$ are contained in a plane. For each event, we define a new coordinate system (x',y',z') by the normal vector on this plane (z'-axis) and the direction of the largest of the three momentum vectors as x'-axis. Three Euler angles ($\psi$,$\theta$,$\phi$) describe the orientation of the (x',y',z')-coordinate system within the laboratory reference system (x,y,z), which is defined by the electric vector of the laser beam (z-axis) and the direction of the neutral beam (x-axis). The spatial orientation of the (x',y',z')-coordinate frame is determined by the spatial anisotropy of the photodissociation process.

The remaining three parameters describe the arrangement of the three momenta in the (x',y')-plane. We introduce the individual fragment energies

$\varepsilon_i = m\mathbf{u}_i^2$ and use the total kinetic energy $W$ and two parameters to show the vector correlation among the fragment momenta within the $(x',y')$ plane.

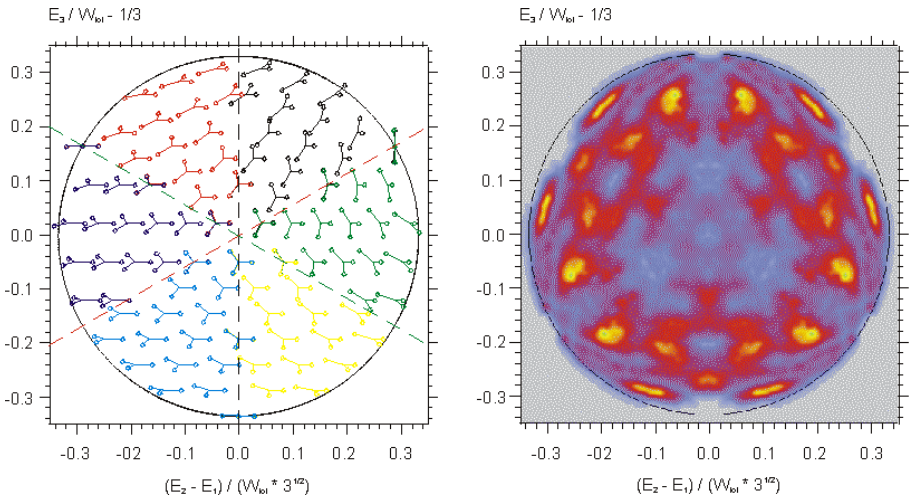


Figure 7: The generalized Dalitz plot on the left shows the correspondence between the location of a data point in the plot and the fragmentation configuration. An experimental distribution of fragmentation vectors is shown on the right (the $3d$E'(1,0){$1,0^0$} state).

This is possible by using a Dalitz plot [18] in which we represent each event by a point in the $(\varepsilon_3/W-1/3)$ vs. $(\varepsilon_1-\varepsilon_2)/(\sqrt{3}\,W)$ plane. Energy and momentum conservation require the data points in this plot to fall inside a circle with radius $1/3$, centered at the origin. In the Dalitz representation the phase space density is conserved. This means that a process with a matrix element independent of the fragmentation configuration leads to a homogeneous distribution in the kinematically allowed circular region. Preferred fragmention pathways can immediately be recognized from the event density in the Dalitz plot as may be seen from Figures 7 and 8.

In Fig. 8 (a) and (b), the triple-coincident events following three-body breakup of the $3s$A$_1$' and $3d$E' Rydberg states (both in their ground vibrational level) are shown in Dalitz plots. Since the three hydrogen atoms are indistinguishable, points are drawn in Fig. 8 for the six permutations of the fragment energies $\varepsilon_i$ measured for each dissociation event.

In order to understand the meaning of the very pronounced islands of correlation appearing in the experimental data in Figures 7 and 8, the geometric and electronic collection efficiency of the detector has to be considered. The efficiency was determined in a Monte Carlo simulation by generating a uniform distribution of fragmentation configurations and calculating the fragment propagation to the detector [31]. Based on these Monte Carlo results, we can definitely exclude experimental artefacts as

contributing to the patterning in the Dalitz maps. Nevertheless, in the figures shown we have corrected the measured distributions by weighting the data points with the geometric collection efficiency.

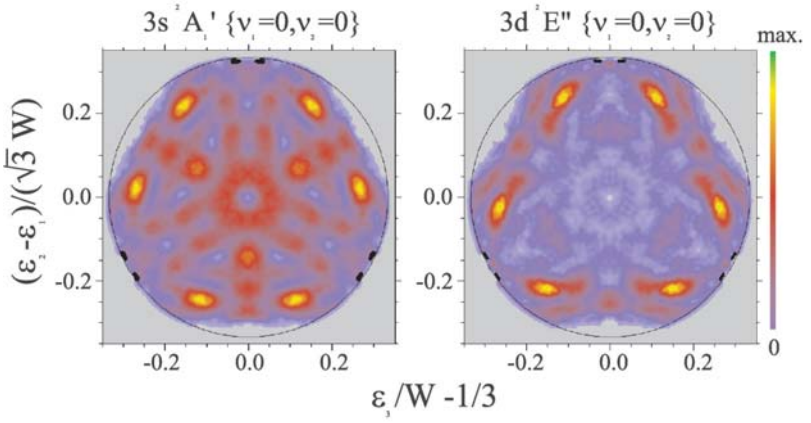


Figure 8: Dalitz plots of the three-body decay of the $3s$A$_1$'(1,0){0,0$^0$} and $3d$E'(1,0){0,0$^0$} initial states of $H_3$. The geometric collection efficiency was calculated by a Monte-Carlo simulation and the measured data were corrected.

Although the initial molecular states are characterized by high symmetry ($D_{3h}$), rather asymmetric fragmentation configurations are much preferred in finding a path into the three-particle continuum. Neither the totally symmetric configuration (center of the plot in Figure 7) nor isosceles configurations (dashed lines in Figure 7, left) show preferred population. It may surprise, that the preferred fragmentation configurations sensitively depend on the initial state. The absolute energies of the states investigated in Figure 8 differ by as little as 75 meV and the nuclear equilibrium configuration for each initial state is extremely close to that of the vibrationless $H_3^+$ ion in its ground electronic state and its lowest rotational level. Since the first publication of such maps [18], these patterns have been studied for about twenty different rovibronic Rydberg-states of $H_3$. Each state shows individual maps with significant vibrational dependence (compare for example Figure 7 with Figure 8b). Also, when comparing maps of $H_3$ and $D_3$ substantial isotope effects are discovered.

The striking difference of the final state distributions in Figure 8a and 8b reflects the different coupling mechanism active between the initial state and the two sheets of the repulsive ground state potential energy surface. In these two cases nearly identical vibrational wavepackets attempt to access the continuum, at nearly equal total energy. The suggestion is that the zero point vibration, while exploring practically identical regions of internuclear

configuration, finds individual regions of access to the continuum. This initial correlation among the fragment momentum vectors is propagated into the final state observables seen in the Dalitz plot.

From a symmetry point of view, the breakdown of the Born-Oppenheimer approximation for the $3s\mathrm{A}_1$' state is mediated by the zero-point motion in the degenerate vibration. In case of the $3d$E' state, the coupling is induced by the rotational tumbling motion [17]. In a semi-classical picture, the vibrational motion explores on a very short time scale the geometries where transitions between the initial state and the ground state surface may occur. Trajectories starting from these geometries interfere, producing a rich pattern in the final state distribution. While the coupling between the bound states and the continuum mediates the first entry of the quasi-bound system into the continuum, a series of avoided crossings between the upper sheet of the repulsive ground state surface and the *s*- and *d*-Rydberg states of $1^2\Sigma_g^+$ symmetry in linear geometry (see Figure 2) will influence the appearance of the continuum state at infinite separation. Efforts are currently being undertaken to interpret the Dalitz maps in terms of the non-adiabatic couplings between the Rydberg states and the neutral continuum [32].

# 4. CONCLUSIONS

The investigation of the dynamics of state-selected neutral states of $H_3$ reveal complex patterns of preferred predissociation. Most notable is an apparently irregular dependence of the predissociation rate on the energy and on the rovibronic nature of the state. These details have currently no firm theoretical understanding. For numerous predissociated states of $H_3$ a complete microscopic view of the half collision from a well characterized initial state to the momentum set of the three correlated ground state hydrogen atoms at infinite separation has been obtained with the Freiburg coincidence spectrometer [18,31]. In the case of DR a Dalitz-type map was recently also obtained [33]. The map obtained in DR is the superposition from a multitude of electronic and rotational angular momenta of the $e+H_3^+$ complex formed as intermediate, even if the rovibrational state of $H_3^+$ is well defined. The state-selective information provided in our half collision approach is a stringent test of the quality of any theoretical treatment of the $e+H_3^+$ problem. It is also a test to its applicability to predict a reliable DR cross section. We are confident that the unrestricted approach to this problem, currently explored by Tashiro and Kato [34], will be able to account for all experimental details documented for this fundamental system of three protons and three electrons.

Acknowledgement: This research was supported through generous funding by the Deutsche Forschungsgemeinschaft in the Sonderforschungsbereich SFB276, TP-C13.

## REFERENCES

[1] G. Herzberg, J. Chem. Phys. **68**, 5298 (1978).
[2] I. Dabrowski and G. Herzberg, Can. J. Phys. **58**, 1238 (1980).
[3] H. Helm, Phys. Rev. Lett. **56**, 42 (1986), Phys. Rev. A **38**, 3425 (1988).
[4] J. K. G. Watson, in *From Atoms to Polymers: Isolelectronic Analogues*, Vol. **11** chap. 4 edited by J.F. Liebman and A. Greenberg, VCH Publishers (1989).
[5] M. C. Bordas, P. C. Cosby, and H. Helm, J. Chem. Phys. **93**, 6303 (1990).
[6] A. Dodhy, W. Ketterle, H. Messmer, and H. Walther, Chem. Phys. Lett. **151**, 133 (1989).
[7] W. Ketterle, H.-P. Messmer, and H. Walther, Europhys. Lett. **8**, 333 (1989).
[8] L. J. Lembo and H. Helm, Chem. Phys. Lett. **163**, 425 (1989).
[9] L. J. Lembo, H. Helm and D. L. Huestis, J. Chem. Phys. **90**, 529 (1989).
[10] L. J. Lembo, C. Bordas, and H. Helm, Phys. Rev. A, **42**, 6660 (1990).
[11] C. Bordas, L. J. Lembo, and H. Helm, Phys. Rev. A, **44**, 1817 (1991).
[12] C. Bordas and H. Helm, Phys. Rev. A **45**, 387 (1992), A **47**, 1209 (1993).
[13] C. Bordas and H. Helm, Phys. Rev. A **43**, 3645 (1991).
[14] I. Mistrik *et al.*, Phys. Rev. A **61**, 033410 (2000).
[15] P. C. Cosby and H. Helm, Phys. Rev. Lett. **61**, 298 (1988).
[16] U. Müller and P. C. Cosby, J. Chem. Phys. **105**, 3532 (1996).
[17] U. Müller and P. C. Cosby, Phys. Rev. A **59**, 3632 (1999).
[18] U. Müller, Th. Eckert, M. Braun and H. Helm, Phys. Rev. Lett. **83**, 2718 (1999).
[19] R. Reichle, I. Mistrik, U. Müller and H. Helm, Phys. Rev. A **60**, 3929 (1999).
[20] J. A. Stephens and C. H. Greene, J. Chem. Phys. **102**, 1579 (1995).
[21] H. Helm, in *Dissociative Recombination: Theory, Experiment and Applications*, edited by B. R. Rowe, A. Mitchell, A. Canosa, (Plenum Press N.Y. 1993) p. 145-153.
[22] M. J. Jensen *et al.*, Phys. Rev. A **63** 052701 (2001).
[23] I. F. Schneider, M. Larsson, A. E. Orel and A. Suzor-Weiner, in *Dissociative recombination: Theory, Experiments and Applications IV*, Edited by M. Larsson, J. B. A. Mitchell and I. F. Schneider, World Scientific (1999), p. 131-141.
[24] V. Kokoouline, C. H. Greene, and B. D. Esry, Nature **412**, 891 (2001).
[25] K. Kaufmann, M. Jungen, and H.-J. Werner, J. Phys. Chem. **87**, 3806 (1983).
[26] J. K. G. Watson *et al.*, Can. J. Phys. **62**, 1875 (1984).
[27] I. D. Petsalakis, G. Theodorakopoulos, and J. S. Wright, J. Chem. Phys. **89**, 6850 (1988).
[28] J. T. Hougen, J. Chem. Phys. **37**, 1433 (1962).
[29] I. Mistrik, R. Reichle, H. Helm, and U. Müller, Phys. Rev. A **63**, 042711 (2001).
[30] I. F. Schneider and A. E. Orel, J. Chem. Phys., **111**, 5873 (1999).
[31] U. Galster *et al.*, accepted for publication in Europ. J. Phys. B (2002).
[32] U. Müller *et al.*, in preparation.
[33] D. Strasser *et al.*, Phys. Rev. Lett. **86**, 779 (2001).
[34] M. Tashiro and S. Kato, this volume page xxx.